Origins of the changing detector response in small megavoltage photon radiation fields

John D. Fenwick[1,2,*], Georgios Georgiou[2,3], Carl G. Rowbottom[2,3], Tracy S. A. Underwood[4], Sudhir Kumar[5] and Alan E. Nahum[6]

1. Department of Molecular and Clinical Cancer Medicine, Institute of Translational Medicine, University of Liverpool. The Sherrington Building, Ashton Street, Liverpool L69 3BX, UK

2. Department of Physics, Clatterbridge Cancer Centre, Clatterbridge Road, Wirral CH63 4JY, UK

3. Department of Physics, University of Liverpool, Oliver Lodge Laboratory, Oxford Street, Liverpool L69 7ZE, UK

4. Department of Medical Physics and Biomedical Engineering, University College London, London WC1E 6BT, UK

5. Radiological Physics and Advisory Division, Bhabha Atomic Research Centre, CT & CRS Building, Anushaktinagar, Mumbai 400094, India

6. Visiting Professor, Department of Physics, University of Liverpool; and 12 Beech House, Ancastle Green, Henley-on-Thames, South Oxfordshire RG9 1UL, UK

[†] Corresponding author, email john.fenwick@liverpool.ac.uk, telephone 0151 556 5091

Key words: small field, detector response, density, atomic number, Monte Carlo

This manuscript comprises 30 pages, including 6 figures and 5 tables

Abstract

Differences in detector response between measured small fields, f_{clin}, and wider reference fields, f_{msr}, can be overcome by using correction factors $k_{Q_{clin},Q_{msr}}^{f_{clin},f_{msr}}$ or by designing detectors with field-size invariant responses. The changing response in small fields is caused by perturbations of the electron fluence within the detector sensitive volume. For solid-state detectors, it has recently been suggested that these perturbations might be caused by the non-water-equivalent effective atomic numbers Z of detector materials, rather than by their non-water-like densities. Using the EGSnrc Monte Carlo code we have analyzed the response of a PTW 60017 diode detector in a 6 MV beam, calculating the $k_{Q_{0.5,4\ cm}}^{0.5,4\ cm}$ correction factor from computed doses absorbed by water and by the detector sensitive volume in 0.5×0.5 and 4×4 cm^2 fields. In addition to the 'real' detector, fully modelled according to the manufacturer's blue-prints, we calculated doses and $k_{Q_{0.5,4\ cm}}^{0.5,4\ cm}$ factors for a '$Z{\rightarrow}$water' detector variant in which mass stopping-powers and microscopic interaction coefficients were set to those of water while preserving real material densities, and for a 'density$\rightarrow$1' variant in which densities were set to 1 g cm^{-3}, leaving mass stopping-powers and interaction coefficients at real levels. $k_{Q_{0.5,4\ cm}}^{0.5,4\ cm}$ equalled 0.910 ± 0.005 (2 standard deviations) for the real detector, was insignificantly different at 0.912 ± 0.005 for the '$Z{\rightarrow}H_2O$' variant, but equalled 1.012 ± 0.006 for the 'density$\rightarrow$1' variant. For the 60017 diode in a 6 MV beam, then, $k_{Q_{0.5,4\ cm}}^{0.5,4\ cm}$ was determined primarily by the detector's density rather than its atomic composition. Further calculations showed this remained the case in a 15 MV beam. Interestingly, the sensitive volume electron fluence was perturbed *more* by detector atomic composition than by density; however, the density-dependent perturbation varied with field-size, whereas the Z-dependent perturbation was relatively constant, little affecting $k_{Q_{0.5,4\ cm}}^{0.5,4\ cm}$.

1. Introduction

Radiation doses absorbed by water from small megavoltage photon fields can be measured using ionization chambers and diamond and diode detectors (Bassinet *et al* 2103, De Coste *et al* 2017). These dosimeters are built from materials whose atomic compositions and densities differ from those of water, and in small fields they may under- or over-respond compared to their readings in the wider ($\geq 4 \times 4 \text{cm}^2$) reference fields in which they are calibrated (McKerracher and Thwaites 1999, Francescon *et al* 2011, Scott *et al* 2012, Underwood *et al* 2013a, Looe *et al* 2015). Doses in small fields can also be measured using radiochromic film, which offers very good resolution and a response that varies little between small and wide fields (Bassinet *et al* 2013, Morales *et al* 2016). However, radiochromic film requires skilled handling and processing, and is not used so widely as more easily operated detectors such as diodes.

A formalism proposed by Alfonso *et al* (2008) and developed in a recent IAEA code of practice (2017) accounts for changes in detector response in small fields by calculating the dose $D_{w\text{-}point}$ in water at the measurement point in a field f_{clin} of quality Q_{clin} as

$$\left(D_{w-point}\right)^{f_{clin}}_{Q_{clin}} \;=\; M^{f_{clin}}_{Q_{clin}} \; N^{f_{msr}}_{Q_{msr}} \; k^{f_{clin},f_{msr}}_{Q_{clin},Q_{msr}} \tag{1}$$

where M is the reading of a detector positioned so that the centre of its sensitive volume lies at the measurement point in water, N is the absorbed dose to water calibration coefficient obtained for the detector in a machine-specific reference field f_{msr} of beam quality Q_{msr}, and k is a correction factor that accounts for the difference in detector response between the measured and reference fields.

In principle, k can be obtained directly from the equation

$$k^{f_{clin},f_{msr}}_{Q_{clin},Q_{msr}} \;=\; \left(\left(D_{w-point}\right)^{f_{clin}}_{Q_{clin}} \big/ \; M^{f_{clin}}_{Q_{clin}} \right) \big/ \left(\left(D_{w-point}\right)^{f_{msr}}_{Q_{msr}} \big/ \; M^{f_{msr}}_{Q_{msr}} \right) \tag{2}$$

by accurately determining doses in water at the measurement point using a dosimeter whose response is largely invariant with field-size, such as radiochromic film (Bassinet *et al* 2013, Morales *et al* 2016). More commonly, k is calculated using Monte Carlo radiation transport calculations, replacing the meter readings in equation (2) with calculated mean doses $\overline{D}_{det}$ in the detector sensitive volume (assuming detector readings scale with $\overline{D}_{det}$),

and taking $D_{w\text{-}point}$ values as doses calculated in a very small voxel of water located within the water phantom in the absence of the detector, the voxel centre lying at the measurement point (Francescon *et al* 2011).

Bouchard *et al* (2009) extended an ionization chamber dosimetry protocol to describe detector response in locations where the in-water radiation fluence varies non-standardly across the region in which the detector is to be placed. This approach allows the average dose absorbed by the sensitive volume from a field *f* of quality Q_f to be converted to dose in water at the measurement point via the equation

$$\{ D_{w-point} / \overline{D}_{det} \}_{Q_f}^{f} \;=\; \{ P_Z \; P_\rho \; P_{vol} \; [\overline{L}_\Delta/\rho]_{det}^{w} \}_{Q_f}^{f} \tag{3}$$

Here the P_Z and P_ρ factors account for the perturbing effects on the electron fluence within the sensitive volume of differences between detector materials and water in atomic number Z and density ρ respectively, while P_{vol} accounts for averaging of the unperturbed fluence across the sensitive volume (Fenwick *et al* 2013). $[\overline{L}_\Delta/\rho]_{det}^{w}$ is the water-to-detector restricted mass electronic stopping-power ratio with a cut-off energy Δ of 10 keV, averaged over the spectrum of electrons energized by the photon beam at the measurement point in water in the absence of the detector. The P_Z factor was denoted as P_{fl} in the formalisms of Bouchard *et al* (2009) and Fenwick *et al* (2013), but is renamed here for clarity.

The P_Z, P_ρ and P_{vol} factors in equation (3) act sequentially as shown in Figure 1, and are given by

$$P_Z^f \;=\; \{ \overline{D}_{det-Z \to H_2O} / (\overline{D}_{det} \; [\overline{L}_\Delta/\rho]_{det}^{w}) \}_{Q_f}^{f} \tag{4}$$

$$P_\rho^f \;=\; \{ \overline{D}_{w-sensvol} / \overline{D}_{det-Z \to H_2O} \}_{Q_f}^{f} \tag{5}$$

$$P_{vol}^f = \{ D_{w-point} / \overline{D}_{w-sensvol} \}_{Q_f}^{f} \tag{6}$$

where $\overline{D}_{det-Z \to H_2O}$ is the dose in the sensitive volume of a detector whose geometry and component densities match those of the original detector but whose microscopic radiation cross-sections and mass stopping-powers match those of unit density (1 g cm^{-3}) water, and $\overline{D}_{w-sensvol}$ is the dose absorbed, in the absence of the detector, by a co-located volume of water having the same dimensions as the detector sensitive volume.

Combining equations (2) and (3), the small field correction factor *k* works out as

$$k_{Q_{clin},Q_{ref}}^{f_{clin},f_{ref}} = \frac{\left\{ P_Z \ P_\rho \ P_{vol} \ [\bar{L}_\Delta/\rho]_{det}^w \right\}_{Q_{clin}}^{f_{clin}}}{\left\{ P_Z \ P_\rho \ P_{vol} \ [\bar{L}_\Delta/\rho]_{det}^w \right\}_{Q_{msr}}^{f_{msr}}} \tag{7}$$

For detectors made from air, silicon and diamond, changes in $[\bar{L}_\Delta/\rho]_{det}^w$ between fields of size 0.5×0.5 and 4×4 cm^2 have been calculated to be 0.2-0.6% (Scott *et al* 2008, Ding and Ding 2012, Czarnecki and Zink 2013, Fenwick *et al* 2013), allowing equation (4) to be approximated as

$$k_{Q_{clin},Q_{ref}}^{f_{clin},f_{ref}} \approx \frac{\left\{ P_Z \ P_\rho \ P_{vol} \right\}_{Q_{clin}}^{f_{clin}}}{\left\{ P_Z \ P_\rho \ P_{vol} \right\}_{Q_{msr}}^{f_{msr}}} \tag{8}$$

Andreo and Benmakhlouf (2017, pp 1526 and 1531) have recently raised two concerns about the formalism of equations (3,7,8) in the context of solid-state detectors –

I. That the 'density perturbation factor' should in fact be understood in terms of the reduced mass electronic stopping-powers of solid-state detector components relative to water, due primarily to differences in *I*-values between component materials and water, and secondarily to differences in electronic density.

II. That attribution of changes in detector response in small photon radiation fields directly to the mass densities of detector components reflects an incomplete interpretation of the physics of relevant radiation interaction processes, which depend strongly on the atomic composition of detector components.

To illustrate their concerns, Andreo and Benmakhlouf provided a simplified expression for the mass electronic stopping-power S_{el}/ρ of electrons

$$\frac{S_{el}}{\rho} \propto \frac{Z}{A} \frac{1}{\beta^2} \left(\zeta(E_k) - lnI - \delta\left(I^2, \rho\frac{Z}{A}, \beta\right) \right) \tag{9}$$

in which β is the electron velocity normalized to light-speed, I and (Z/A) denote the mean excitation energy and ratio of atomic to mass numbers of the atoms in the medium traversed, ζ is a term that varies with electron kinetic energy E_k, δ describes the polarization effect, and the *lnI* term is doubled when δ is conventionally defined (see Heitler 1954, ICRU 1984, Sternheimer *et al* 1984 and Attix 1986 for background). For the electrons ionized in radiotherapy photon beams, the polarization effect causes S_{el}/ρ to be a few per cent lower

in condensed media than in gases, the reduction being greater at higher electron energies. S_{el}/ρ is also lower

for elements with higher atomic numbers and correspondingly higher I-values than it is for lighter elements.

Consequently S_{el}/ρ values are 2-35% less for silicon than for graphite, diamond, air or water at relevant electron

energies.

Thus, Andreo and Benmakhlouf (2017) apparently hypothesize that the variation of solid-state detector

response with field-size is driven by differences in S_{el}/ρ between detector materials and water, rather than by

fluence perturbations caused directly by differences in density. A corollary is that a '$Z{\rightarrow}H_2O$' detector made

from fictitious materials, all having the same S_{el}/ρ and microscopic radiation interaction cross-sections as unit

density water but the densities of real materials, should have k factors of 1 in all fields in which the volume-

averaging factor P_{vol} negligibly differs from unity. A further corollary is that a 'density$\rightarrow$1'detector built of

fictitious materials having unit densities, but with S_{el}/ρ and microscopic cross-section values corresponding to

real materials, should have just the same k values as a detector built from the real substances.

In this work, we test this hypothesis using fictitious materials created within a Monte Carlo radiation transport

code. Specifically, we model the response of the widely used PTW 60017 diode detector (PTW, Freiburg,

Germany), initially building the real detector *in-silico* from its real components according to manufacturer

blue-prints, and then building $Z{\rightarrow}H_2O$ and density$\rightarrow$1 variants of the detector from correspondingly modified

materials. We compute doses delivered to water and to the sensitive volumes of the real, $Z{\rightarrow}H_2O$ and

density$\rightarrow$1 detector variants in different fields, and from these we calculate detector k correction factors along

with P_Z, P_ρ and P_{vol} factors, and determine the influence on k factors of density versus mass stopping-powers

and microscopic cross-sections.

2.   Methods

Monte Carlo studies of the response of the PTW 60017 diode detector were carried out using the EGSnrc

system (Kawrakow *et al* 2011) run on a 64 core AMD 6378 Opteron-based computer. The detector was built

in the EGS++ geometry package within the egs_chamber code (Wulff *et al* 2008) according to the

manufacturer's technical drawings: its silicon sensitive region has a cross-sectional area of 1 mm^2, a thickness

of 30 μm, density 2.3 g cm^{-3} and atomic number 14. PEGS4 input files were initially created for all the real

constituent materials of the detector using the EGSnrcMP package (Kawrakow *et al* 2006, Kawrakow *et al* 2011), setting the AP and AE thresholds for secondary bremsstrahlung photons and knock-on electrons to 1 and 512 keV (total energy) respectively. The resulting detector model has been validated against experimental data (Underwood *et al* 2015a). A $Z \rightarrow H_2O$ 60017 detector was built using the same geometry together with PEGS4 files modified by setting the stopping-powers and microscopic cross-sections of the component materials to those of unit density water, but keeping densities at the real material levels. And a density$\rightarrow$1 detector was similarly created by setting all densities to 1 g cm^{-3} in the PEGS4 files while keeping mass stopping-powers and microscopic cross-sections at the real material levels (Figure 2).

Detector dose calculations were carried out using the egs_chamber code (Wulff *et al* 2008), with input phase-space files obtained from an experimentally validated Varian Clinac iX 6 MV beam model (Varian Medical Systems, Palo Alto, California) created using the BEAMnrc system (Rogers *et al* 2011a) as described by Underwood *et al* (2013b). Monte Carlo settings included the modelling of Compton interactions for bound electrons, Rayleigh scattering, atomic relaxation events, and relativistic spin effects in the multiple scattering of charged particles. Electron impact corrections were switched on. Photon interaction cross-sections were taken from the XCOM database (Berger et al 2010), and cross-sections used to sample photon energies in bremsstrahlung events were taken from the NIST databases (Hubbell and Seltzer 2004). The electron and photon cut-off parameters ECUT and PCUT were set to 521 and 1 keV.

Sensitive volume doses $\overline{D}_{det}$, $\overline{D}_{det-Z \rightarrow H_2O}$ and $\overline{D}_{det-density \rightarrow 1}$ were calculated for the real, $Z \rightarrow H_2O$ and density$\rightarrow$1 detectors in 0.5×0.5 and 4×4 cm^2 fields defined by the linear accelerator (linac) jaws, using phase-space files containing 2.9×10^7 and 1.4×10^9 particles. The detectors were aligned parallel to the beam and positioned on-axis with their sensitive volumes at 5 cm depth in a 1 m^3 water-tank located at 100 cm source-to-surface distance (SSD). The doses were normalized to the number of electrons incident on the linac target, and calculated with a statistical precision of better than $\pm$ 0.4% (2 standard deviations, s.d.) by running 1.5×10^8 and 1.5×10^9 particle histories in the two fields. To speed up the calculations 128-fold cross-sectional enhancement was turned on within a shell extending 2 cm beyond the sensitive volume (Wulff *et al* 2008).

Point doses $D_{w\text{-}point}$ absorbed by water in the absence of the 60017 detector were calculated using the DOSXYZnrc code (Rogers *et al* 2011a). For the 0.5×0.5 cm^2 field $D_{w\text{-}point}$ was calculated for a small water voxel of lateral dimensions 0.25×0.25 mm^2 and thickness 0.5 mm whose centre lay on-axis at 5 cm depth in the water-tank. For computational efficiency a wider 2×2×0.5 mm^3 voxel was used to calculate $D_{w\text{-}point}$ in the 4×4 cm^2 field, since the fluence profile is flat at the centre of this field. Mean doses $\overline{D}_{w-sensvol}$ absorbed from the 0.5×0.5 and 4×4 cm^2 fields by a cylindrical water voxel whose centre was co-located with the point-like voxel, and whose lateral dimensions matched the 1 mm^2 cross-sectional area of the 60017 sensitive volume, were calculated using the CAVRZnrc code (Rogers *et al* 2011b). A voxel thickness of 0.5 mm, 17 times that of the detector sensitive volume, was used for efficiency since at megavoltage energies doses vary little with depth in water on sub-millimetre length-scales.

From equation (2) and the $D_{w\text{-}point}$, $\overline{D}_{det}$, $\overline{D}_{det-Z \rightarrow H_2O}$ and $\overline{D}_{det-density \rightarrow 1}$ doses computed for the 0.5×0.5 cm^2 and 4×4 cm^2 fields, correction factors $k_{Q_{0.5,4\text{ cm}}}^{0.5,4\text{ cm}}$ were calculated for the 60017 detector and its $Z \rightarrow H_2O$ and density→1 variants. These factors represent the corrections required if the detectors are used to measure dose on-axis in the 0.5×0.5 cm^2 field relative to dose in an intermediate 4×4 cm^2 field (IAEA, 2017).

Values of P_Z and P_ρ were calculated for the 60017 diode in the 0.5×0.5 and 4×4 cm^2 fields using equations (5) and (6) together with computed $\overline{D}_{w-sensvol}$, $\overline{D}_{det-Z \rightarrow H_2O}$ and $\overline{D}_{det}$ doses, and the water-to-silicon restricted stopping-power ratio $[\overline{L}_\Delta / \rho]_{Si}^w$ averaged over the in-water electron fluence spectrum in the cylindrical water voxel of 1 mm^2 cross-section. The stopping-power ratio was computed using the SPRRZnrc code (Rogers *et al* 2011b) with a cut-off energy Δ of 10 keV and including track-end terms. For the 0.5×0.5 cm^2 field, P_{vol} was calculated from $D_{w-point}$ and $\overline{D}_{w-sensvol}$ doses using equation (6).

As well as the 30 μm thick silicon sensitive volume, several other 60017 detector components have non-water-like densities and atomic compositions, including a slab of silicon that underlies the sensitive volume. To determine how the dose absorbed by the sensitive volume is affected by its atomic composition and density, independent of other detector components, we computationally created a bare 60017 detector comprising the silicon sensitive volume alone, surrounded entirely by water (Figure 2), and carried out Monte Carlo calculations for this bare detector and its $Z \rightarrow H_2O$ and density→1 variants. To explore whether these Z and

density dependences of absorbed dose change with the thickness of the sensitive volume, we also created *in-silico* a second 'thicker bare' detector with a much greater thickness of 500 μm but the same lateral dimensions (Figure 2).

Additionally, a 'core' detector was created comprising just the 30 μm thick sensitive volume and regions of the detector lying immediately above and below it. This core detector was surrounded entirely by water and its cross-sectional area was 1 mm^2, matching that of the sensitive volume (Figure 2). Within the sensitive volumes of the core detector and its $Z \rightarrow H_2O$ and density$\rightarrow$1 variants, and within the cylindrical 1 mm^2 cross-section water voxel, total electron (+ positron) fluence spectra differential in energy per source particle, $\phi_{E,core-variant}^f$ and $\phi_{E,w-sensvol}^f$, were computed down to 10 keV using the FLURZnrc code as described by Kumar *et al* (2015). The spectra provide visual summaries of perturbations of the in-water fluence within the sensitive volume.

To further gauge differences between the spectra we calculated the spectral ratios $\phi_{E,w-sensvol}^f / \phi_{E,core}^f$, $\phi_{E,core-Z \rightarrow H_2O}^f / \phi_{E,core}^f$ and $\phi_{E,core-density \rightarrow 1}^f / \phi_{E,core}^f$ for the 0.5×0.5 and 4×4 cm^2 fields. Additionally, we calculated the double ratio $[\phi_{E,core-Z \rightarrow H_2O}^{0.5\,cm} / \phi_{E,core}^{0.5\,cm}] / [\phi_{E,core-Z \rightarrow H_2O}^{4\,cm} / \phi_{E,core}^{4\,cm}]$ which, being the ratio of the total electron fluence spectrum generated in the sensitive volume of the $Z \rightarrow H_2O$ core detector by the 0.5×0.5 cm^2 field to that generated in the real core detector, divided by the same ratio for the 4×4 cm^2 field, is a spectral decomposition of the ratio of P_Z correction factors in the two fields (equation (4)). We also calculated the double ratio $[\phi_{E,w-sensvol}^{0.5\,cm} / \phi_{E,core-Z \rightarrow H_2O}^{0.5\,cm}] / [\phi_{E,w-sensvol}^{4\,cm} / \phi_{E,core-Z \rightarrow H_2O}^{4\,cm}]$, a spectral decomposition of the ratio of P_ρ correction factors in the 0.5×0.5 and 4×4 cm^2 fields (equation (6)).

Finally, to check the generalizability of the results obtained for the 60017 diode aligned with the beam axis in jaw-defined 6 MV 0.5×0.5 and 4×4 cm^2 fields, we carried out calculations for the same detector in three further circumstances –

i.   Aligned with the beam axis at 5 cm depth in a 6 MV 0.7×0.7 cm^2 field. From the computed sensitive volume doses and the dose delivered to a point-like (0.25^2×0.5 mm^3) water voxel, $k_{Q_{0.7,4\,cm}}^{0.7,4\,cm}$ factors were calculated.

ii.   Angled at 45° to the beam axis, at 5 cm depth in the 6 MV 0.5×0.5 and 4.0×4.0 cm^2 fields. From the computed sensitive volume doses, $k_{Q_{0.5,4\,\text{cm}}}^{0.5,4\,\text{cm}}(45°)$ factors were calculated, describing the corrections required when dose is measured in the 0.5×0.5 cm^2 field relative to the 4×4 cm^2 field with the detector set at 45° to the beam axis in both fields.

iii. Aligned with the beam axis, at 5 cm depth in 15 MV 0.5×0.5 and 4×4 cm^2 fields, using input phase-space files obtained from an experimentally validated model of a Varian 2100C 15 MV beam (Scott *et al* 2008) and comprising 6.7×10^6 and 3.6×10^8 particles for the two fields. From the computed sensitive volume doses together with point-like water voxel doses, 15 MV beam $k_{Q_{0.5,4\,\text{cm}}}^{0.5,4\,\text{cm}}$ factors were calculated.

3.   Results

Calculated doses absorbed from the 6 MV 0.5×0.5 and 4×4 cm^2 fields by the sensitive volumes of the real, $Z\rightarrow$ H$_2$O and density$\rightarrow$1 variants of the bare, thicker bare, core and full PTW 60017 diode detectors, aligned with the beam axis, are listed in Table 1. Doses delivered to water voxels in the absence of the detectors are listed in Table 2, together with restricted water-to-silicon stopping-power ratios averaged over the electron fluence spectra generated by these fields in the 1 mm^2 cross-section cylindrical water voxel.

The 6 MV $k_{Q_{0.5,4\,\text{cm}}}^{0.5,4\,\text{cm}}$ correction values calculated for the different detectors from these doses are listed in Table 3 and plotted in Figure 3a. Three patterns are evident. Firstly, the values decrease progressively as more components are added to the detector model: $k_{Q_{0.5,4\,\text{cm}}}^{0.5,4\,\text{cm}}$ is 1.002 ± 0.006 (2 s.d.) for the bare real detector comprising the 30 μm thick sensitive volume alone, but falls to 0.910 ± 0.005 for the fully modelled real detector. Secondly, no significant differences exist between $k_{Q_{0.5,4\,\text{cm}}}^{0.5,4\,\text{cm}}$ values calculated for the real detectors and for their $Z\rightarrow$ H$_2$O counterparts, in which component mass stopping-powers and microscopic cross-sections were changed to those of water but real densities were retained. And thirdly, for the density$\rightarrow$1 detector variants, in which component densities were modified to that of water but real mass-stopping powers and microscopic cross-sections were retained, $k_{Q_{0.5,4\,\text{cm}}}^{0.5,4\,\text{cm}}$ values lie in the range 1.000 ± 0.006 to 1.013 ± 0.005. These values are little different to the P_{vol} correction factor value of 1.006 ± 0.004 that can be calculated from

the 0.5×0.5 cm^2 field in-water doses listed in Table 2, and which accounts for dose averaging of the unperturbed radiation fluence across the sensitive volume.

P_ρ and P_Z perturbation correction factors calculated from data in Tables 1 and 2 for the 6 MV beam are listed in Table 4 and plotted in Figure 4. For the 0.5×0.5 cm^2 field, values of both factors progressively decrease as more detector components are added: for the bare detector $P_\rho^{0.5\ cm}$ and $P_Z^{0.5\ cm}$ are 1.000 ± 0.002 and 0.954 ± 0.002 respectively, falling to 0.906 ± 0.002 and 0.865 ± 0.002 for the fully modelled detector. For the 4×4 cm^2 field, however, all $P_\rho^{4\ cm}$ values lie very close to 1 whereas $P_Z^{4\ cm}$ values differ insignificantly from those calculated for the 0.5×0.5 cm^2 field.

Figures 5(a) and 5(b) show the calculated total electron (+ positron) fluence spectra per MeV per source particle generated by the 6 MV 0.5×0.5 and 4×4 cm^2 fields within the 1 mm^2 cylindrical cross-section water voxel in the absence of a detector, and within the sensitive volumes of the real, $Z{\rightarrow}H_2O$ and density$\rightarrow$1 variants of the core detector. For the 0.5×0.5 cm^2 field, the fluence spectrum in the $Z{\rightarrow}H_2O$ detector variant lies much closer to the in-water spectrum than does the spectrum in the density$\rightarrow$1 detector variant, which is closer to the spectrum in the real detector. This is further illustrated by the ratios $\phi_{E,w-sensvol}^{0.5\ cm}/\phi_{E,core}^{0.5\ cm}$, $\phi_{E,core-Z{\rightarrow}H_2O}^{0.5\ cm}/\phi_{E,core}^{0.5\ cm}$ and $\phi_{E,core-density{\rightarrow}1}^{0.5\ cm}/\phi_{E,core}^{0.5\ cm}$ plotted in Figure 5(c). In the 4×4 cm^2 field, the fluence spectrum in the sensitive volume of the $Z{\rightarrow}H_2O$ variant of the core detector also lies much closer to the in-water spectrum than does the spectrum in the density$\rightarrow$1 variant, which again is closer to the spectrum in the real detector (Figures 5(b) and 5(d)). In fact, in the 4×4 cm^2 field the in-water and $Z{\rightarrow}H_2O$ fluence spectra are almost indistinguishable.

The double-ratio $[\phi_{E,core-Z{\rightarrow}H_2O}^{0.5\ cm}/\phi_{E,core}^{0.5\ cm}]/[\phi_{E,core-Z{\rightarrow}H_2O}^{4\ cm}/\phi_{E,core}^{4\ cm}]$ is plotted in Figure 6(a). Its values range from 0.96 to 1.03 and oscillate around 1.00, in line with the close match between the P_Z values calculated for the core detector in the 0.5×0.5 and 4×4 cm^2 fields, the double-ratio being a spectral decomposition of the ratio of P_Z factors in these fields. The double-ratio $[\phi_{E,w-sensvol}^{0.5\ cm}/\phi_{E,core-Z{\rightarrow}H_2O}^{0.5\ cm}]/[\phi_{E,w-sensvol}^{4\ cm}/\phi_{E,core-Z{\rightarrow}H_2O}^{4\ cm}]$ is plotted in Figure 6(b). Its values lie predominantly below 1.00, most often between 0.95-0.98, in line with

the 0.96 ratio of core detector P_ρ values in the 0.5×0.5 and 4×4 cm^2 fields since this double-ratio is a spectral decomposition of the ratio of P_ρ factors in these fields.

Calculated doses absorbed from a 0.7×0.7 cm^2 field by the sensitive volumes of the real, $Z{\rightarrow}H_2O$ and density$\rightarrow$1 variants of the full 60017 detector aligned with the axis of the 6 MV beam are listed in Table 5, together with the doses delivered to a point-like water voxel in the absence of the detector. Sensitive volume doses absorbed from 0.5×0.5 and 4.0×4.0 cm^2 fields when the detector is oriented at 45° to the 6 MV beam axis are also listed in the table, as are sensitive volume and point-like water voxel doses absorbed from 15 MV 0.5×0.5 and 4.0×4.0 cm^2 fields when the detector is aligned with the beam axis.

Values of the 6 MV $k_{Q_{0.7,4\,cm}}^{0.7,4\,cm}$, 6 MV $k_{Q_{0.5,4\,cm}}^{0.5,4\,cm}(45°)$ and 15 MV $k_{Q_{0.5,4\,cm}}^{0.5,4\,cm}$ correction factors calculated from these doses for the full 60017 diode detector and its $Z{\rightarrow}H_2O$ and density$\rightarrow$1 variants are listed in Table 3 and plotted in Figure 3b. Similarly to the 6 MV $k_{Q_{0.5,4\,cm}}^{0.5,4\,cm}$ factors, there is little difference between values of these factors calculated for the real and $Z{\rightarrow}H_2O$ detector variants, whereas values calculated for the density$\rightarrow$1 variant lie close to 1.000, in the range 1.000-1.010 ± 0.006.

4. Discussion

We have calculated very similar 6 MV $k_{Q_{0.5,4\,cm}}^{0.5,4\,cm}$ values for the full, bare, thicker bare and core versions of the 60017 detector aligned with the beam axis (0.910, 0.965, 0.978 and 1.002 respectively) and for their $Z{\rightarrow}$water variants (0.912, 0.967, 0.975, 1.006). This near-equivalence reflects the close similarities reported by Scott *et al* (2012, Figure 2) between the responses of simplified models of a PTW diamond detector, a PTW 31016 Pinpoint detector and a Scanditronix unshielded diode (Scanditronix-Wellhöfer, Uppsala, Sweden) and their $Z{\rightarrow}H_2O$ variants in a 15 MV beam.

On the other hand, for the density$\rightarrow$1 variants of the full, bare, thicker bare and core 60017 detectors, we calculated 6 MV $k_{Q_{0.5,4\,cm}}^{0.5,4\,cm}$ values of 1.000-1.013, all close to the value of one that would be obtained for an ideal point-like water-equivalent detector, and very close to the 1.006 P_{vol} factor that accounts for averaging of the unperturbed in-water electron fluence across the finite detector sensitive volume in the 6 MV 0.5×0.5

cm^2 field. For the 60017 detector, then, $k_{Q_{0.5,4 \text{ cm}}}^{0.5,4 \text{ cm}}$ values change far more in response to detector density modifications than to atomic number modifications. At first sight this is surprising, because we also found that the calculated total electron fluence within the sensitive volume of the detector was perturbed more by differences between the atomic compositions of detector components and water than by differences in density (Table 4, Figure 5), reflecting similar results reported by Benmakhlouf and Andreo (2017, Figure 6) for the bare sensitive volume of an IBA EFD diode detector in a 0.5×0.5 cm^2 field.

To understand why the $k_{Q_{0.5,4 \text{ cm}}}^{0.5,4 \text{ cm}}$ value calculated for the 60017 detector is influenced much more by the densities of its components than by their atomic numbers, despite atomic number more greatly perturbing electron fluence, it is useful to recall that $k_{Q_{0.5,4 \text{ cm}}}^{0.5,4 \text{ cm}}$ accounts for the *difference* in detector response between the 0.5×0.5 and 4×4 cm^2 fields (equation (1)). Consequently, $k_{Q_{0.5,4 \text{ cm}}}^{0.5,4 \text{ cm}}$ is driven by the *difference* between fluence perturbations in these fields rather than by the absolute level of effect in either field. It can readily be seen from Figure 5 that the fluence spectrum within the detector sensitive volume is affected more by the $Z \rightarrow H_2O$ modification of detector mass stopping-powers and microscopic cross-sections than by the density$\rightarrow 1$ modification. However, it is apparent in Figure 6 that the $Z\rightarrow$water changes in fluence spectra are similar in 0.5×0.5 and 4×4 cm^2 fields, whereas the density$\rightarrow 1$ changes in spectra differ between the two field-sizes and therefore drive $k_{Q_{0.5,4 \text{ cm}}}^{0.5,4 \text{ cm}}$ away from unity.

This effect is further illustrated by the 6 MV P_ρ and P_Z factors listed in Table 4 and plotted in Figure 4. The P_Z values are almost identical in the 0.5×0.5 and 4×4 cm^2 fields, whereas P_ρ values differ significantly between these fields for all the detectors modelled, except for the bare detector whose $k_{Q_{0.5,4 \text{ cm}}}^{0.5,4 \text{ cm}}$ value is insignificantly different from one. Differences between P_ρ values in small and wider fields have been discussed previously (Fenwick *et al* 2012). When a detector with mass stopping-powers and microscopic radiation cross-sections matching those of unit density water is placed in water in fields sufficiently large that the photon fluence is uniform throughout the whole volume of origin of electrons traversing the detector sensitive volume, it follows from Fano's theorem that the electron fluence generated by the photons is independent of density variations. The photon fluence uniformity condition is approximately met in 6 MV 4×4 cm^2 fields, but not in 0.5×0.5 cm^2

fields. The resulting lack of lateral electronic equilibrium in 0.5×0.5 cm^2 fields causes the absorbed dose to rise with increasing detector density, leading to P_ρ correction factors of less than one for detectors denser than water, for example 0.865 ± 0.004 and 0.924 ± 0.003 for the full and thicker bare detectors. For the very thin (30 μm) 60017 detector bare sensitive volume alone, however, we calculated P_ρ and $k_{Q_{0.5,4\,\text{cm}}}^{0.5,4\,\text{cm}}$ values of 1.000 and 1.002 respectively in the 0.5×0.5 cm^2 field, in agreement with a theoretical framework presented by Fenwick et al (2012), in which P_ρ and $k_{Q_{0.5,4\,\text{cm}}}^{0.5,4\,\text{cm}}$ values are expected to differ little from one when the sensitive volume is surrounded entirely by water and the average energy lost by electrons traversing the sensitive volume, filled either with its own medium or water, is much smaller than their mean initial energy.

Viewed from another perspective, the density-dependent electron fluence perturbation that occurs in fields too small to establish lateral electronic equilibrium causes the breakdown of the Bragg-Gray relationship between doses absorbed from these fields by water and by air-filled cavities sufficiently small that the electron fluence entering them is largely unchanged after traversing them (Kumar et al 2015), unless the cavities are so small that the electron fluence remains largely unchanged after crossing them even when they are filled with water.

The $k_{Q_{0.5,4\,\text{cm}}}^{0.5,4\,\text{cm}}$ value of 0.910 calculated in this work for the real PTW 60017 diode in a 6 MV beam is very close to experimental and computational values reported by Underwood et al (2015a, Figure 2) after allowing for a change in calibration field from 10×10 to 4×4 cm^2. Other studies, however, have reported 6 MV $k_{Q_{0.5,4\,\text{cm}}}^{0.5,4\,\text{cm}}$ values of around 0.94 for the 60017 detector (IAEA 2017). The lower value reported here has been independently experimentally validated on a Varian TrueBeam linac in Liverpool, and reflects our use of jaw-defined rather than multileaf-defined fields. Underwood et al (2015b) measured 10 MV $k_{Q_{0.5,4\,\text{cm}}}^{0.5,4\,\text{cm}}$ factors for jaw- and MLC-defined fields on a TrueBeam linac, and found that the factor was roughly 3% lower for the jaw-defined fields. Similarly, Cranmer-Sargison et al (2013) reported that the 6 MV $k_{Q_{0.5,4\,\text{cm}}}^{0.5,4\,\text{cm}}$ factor for an Elekta MLCi2 multieaf was roughly 2% lower than for an Agility multileaf with a broader penumbra.

The finding that P_Z varies little with field-size, even for detectors such as the 60017 diode built from materials with effective atomic numbers considerably different to water, concurs with recently reported Monte Carlo calculations made for a radiophotoluminescent glass dosimeter (Hashimoto et al, 2018). A brief, tentative

explanation is that fluence perturbations due to changes in electron interactions will be the same for electrons of a specific energy in any field, hence the similarity between the $\left[\phi_{E,core-Z \to H_2O}^{0.5 \text{ cm}} / \phi_{E,core}^{0.5 \text{ cm}} \right]$ curves plotted in Figure 5 for the 0.5×0.5 and 4×4 cm^2 fields. Despite the similarity of these curves, P_Z could differ between the two fields if the relative shapes of their electron fluence spectra varied substantially, since P_Z is a spectral average of the $\left[\phi_{E,core-Z \to H_2O}^{f} / \phi_{E,core}^{f} \right]$ ratio. However, the difference between the shapes of the spectra plotted in Figure 5 for the two fields is insufficient to generate notable differences between their P_Z values.

In an earlier study (Fenwick *et al,* 2013) we found that P_Z values calculated for simplified models of the PTW 31016 Pinpoint 3D ionization chamber and 60003 diamond detector differed little from unity in any field, presumably because the non-water-equivalent volumes of these simplified detectors were quite small, and the mass stopping-powers of air and diamond do not differ greatly from those of water. Consequently, the variation of $k_{Q_{clin},Q_{msr}}^{f_{clin},f_{msr}}$ factors for the simplified detector models was driven largely by density. Here we have found that the variation with field-size of the $k_{Q_{0.5,4 \text{ cm}}}^{0.5,4 \text{ cm}}$ factor of a 60017 diode detector was also largely driven by density, the P_Z factor for this detector varying little with field-size despite being substantially different to one.

Returning to the concerns of Andreo and Benmakhlouf (2017), then, it is clear that the electron fluence in the 60017 diode sensitive volume was perturbed more by the the mass stopping-powers and microscopic interaction coefficients of detector components than by their densities, reflecting similar findings for an IBA EFD diode reported by Benmakhlouf and Andreo (2017). However, the 6 MV $k_{Q_{0.5,4 \text{ cm}}}^{0.5,4 \text{ cm}}$ correction factor results we obtained were the reverse of those expected on the basis of Andreo's and Benmakhlouf's hypothesis that non-unit k factors result from non-water-equivalent mass stopping-powers rather than densities: instead of $Z \to H_2O$ k factors being close to unity and density→1 k factors being similar to those of real detectors, we found density→1 k factors close to unity and $Z \to H_2O$ k factors similar to those of real detectors. Because the density-dependent fluence perturbation varied between fields ≤4×4 cm^2 whereas the larger atomic number-dependent perturbation was relatively constant, the 6 MV $k_{Q_{0.5,4 \text{ cm}}}^{0.5,4 \text{ cm}}$ correction factors varied much more with changes in detector density than with changes in mass stopping-powers and microscopic interaction cross-sections. Likewise, values of 6 MV $k_{Q_{0.7,4 \text{ cm}}}^{0.7,4 \text{ cm}}$, 6 MV $k_{Q_{0.5,4 \text{ cm}}}^{0.5,4 \text{ cm}}(45°)$ and 15 MV $k_{Q_{0.5,4 \text{ cm}}}^{0.5,4 \text{ cm}}$ correction factors

calculated for the 60017 diode detector also depended much more on the densities of detector materials than on their mass stopping-powers.

5.   Conclusions

The electron fluence within the sensitive volume of a PTW 60017 diode detector was perturbed more by differences in atomic number between components of the detector and water than by differences in density. Nevertheless, for this detector departures from unity of the calibration correction factor $k_{Q_{clin},Q_{msr}}^{f_{clin},f_{msr}}$ in small fields were driven by differences in density rather than atomic number. This apparent contradiction arises because $k_{Q_{clin},Q_{msr}}^{f_{clin},f_{msr}}$ accounts for the *difference* in detector response between the small field f_{clin} (eg 0.5×0.5 cm^2) in which a detector is used and in the wider field f_{msr} (eg 4×4 cm^2) in which it is calibrated, and consequently reflects the *difference* between the fluence perturbations in the two fields rather than the absolute perturbation in either field. For the 60017 detector, atomic number-related fluence perturbations were very similar in the 0.5×0.5 and 4×4 cm^2 fields but density-related perturbations differed between the two field-sizes, and consequently the non-unity $k_{Q_{0.5,4\,cm}}^{0.5,4\,cm}$ value obtained for the fully modelled detector was driven by the non-water-like densities of its component materials, rather than by their non-water-like atomic compositions. Likewise, values of 6 MV $k_{Q_{0.7,4\,cm}}^{0.7,4\,cm}$ and $k_{Q_{0.5,4\,cm}}^{0.5,4\,cm}(45°)$ factors and 15 MV $k_{Q_{0.5,4\,cm}}^{0.5,4\,cm}$ factors calculated for the detector varied far more in response to changes in detector density than to changes in atomic composition.

References

Alfonso R, Andreo P, Capote R, Saiful Huq M, Kilby W, Kjäll P, Mackie T R, Palmans H, Rosser K, Seuntjens J, Ullrich W and Vatnisky S 2008 A new formalism for reference dosimetry of small and nonstandard fields *Med. Phys.* **35** 5179–86

Andreo P and Benmakhlouf H 2017 Role of the density, density effect and mean excitation energy in solid-state detectors for small photon fields *Phys. Med. Bio*l. **62** 1518-1532

Attix F H 1986 Introduction to Radiological Physics and Radiation Dosimetry (New York: Wiley) pp 165-180

Bassinet C, Huet C, Derreumaux S, Brunet G, Chéa M, Baumann M, Lacornerie T, Gaudaire-Josset S, Trompier F, Roch P, Boisserie G and Clairand I 2013 Small fields output factors measurements and correction factors determination for several detectors for a Cyberknife® and linear accelerators equipped with microMLC and circular cones *Med. Phys.* **40** 071725

Benmakhlouf H and Andreo P 2017 Spectral distribution of particle fluence in small field detectors and its implication on small field dosimetry *Med. Phys.* **44** 713-724

Berger M J, Hubbell J H, Seltzer S M, Chang J, Coursey J S, Sukumar R, Zucker D S, and Olsen K 2010 *XCOM: Photon Cross Section Database (version 1.5) Technical Report* (Gaithersburg, MD: National Institute of Standards and Technology)

Bouchard H, Seuntjens J, Carrier J-F and Kawrakow I 2009 Ionisation chamber gradient effects in nonstandard beam configurations *Med. Phys.* **36** 4654–63

Cranmer-Sargison G, Liu P Z Y, Weston S, Suchowersk N and Thwaites D I 2013 Small field dosimetric characterization of a new 160-leaf MLC *Phys. Med. Biol.* **58** 7343-7354

Czarnecki D and Zink K 2013 Monte Carlo calculated correction factors for diodes and ion chambers in small photon fields *Phys. Med. Biol.* **58** 2431-2444

De Coste V, Francescon P, Marinelli M, Masi L, Paganini L, Pimpinella M, Prestopino G, Russo S, Stravato A, Verona C and Verona-Rinati G 2017 Is the PTW 60019 microDiamond a suitable candidate for small field reference dosimetry? *Phys. Med. Biol.* **62** 7036-7055

Ding G X and Ding F 2012 Beam characteristics and stopping-power ratios of small radiosurgery photon beams *Phys. Med. Biol.* **57** 5509-5521

Fenwick J D, Kumar S, Scott A J D and Nahum A E 2013 Using cavity theory to describe the dependence on detector density of dosimeter response in non-equilibrium small fields *Phys. Med. Biol.* **58** 2901-2923

Francescon P, Cora S and Santariano N 2011 Calculation of $k_{Q(clin),Q(msr)}^{f(clin),f(msr)}$ for several small detectors and for two linear accelerators using Monte Carlo simulations *Med. Phys.* **38** 6513-26

Hashimoto S, Fujita Y, Katayose T, Mizuno H, Saltoh H and Karasawa K 2018 Field-size correction factors for a radiophotoluminescent glass dosimeter for small-field and intensity-modulated radiation therapy beams *Med. Phys*. **45** 382-390

Heitler W 1954 The Quantum Theory of Radiation (Oxford: Clarendon press 3rd Edition, reprinted in 2015 by Dover Publishing of New York)

Hubbell J H and Seltzer S M 2004 *Tables of X-Ray Mass Attenuation Coefficients and Mass Energy-Absorption Coefficients (Version 1.4)* (Gaithersburg, MD: National Institute of Standards and Technology)

IAEA 2017 *Dosimetry of Small Static Fields Used in Radiotherapy: An International Code of Practice for Reference and Relative Dose Determination* Technical Reports Series 483 (Vienna: International Atomic Energy Agency)

ICRU 1984 *Stopping Powers for Electrons and Positrons* ICRU Report 37 (Bethesda MD: International Commission on Radiation Units and Measurements)

Kawrakow I, Mainegra-Hing E and Rogers D W O 2006 *NRCC Report PIRS-877; EGSnrcMP: the multi-platform environment for EGSnrc* (Ottawa: National Research Council of Canada)

Kawrakow I, Mainegra-Hing E, Rogers D W O, Tessier F and Walters B R B 2011 *NRCC Report PIRS-701; The EGSnrc code system: Monte Carlo simulation of electron and photon transport* (Ottawa: National Research Council of Canada)

Kumar S, Fenwick J D, Underwood T S A, Deshpande D D, Scott A J D and Nahum A E 2015 Breakdown of Bragg-Gray behaviour for low-density detectors under electronic disequilibrium conditions in small megavoltage photon fields *Phys. Med. Biol.* **60** 8187-8212

Looe H K, Harder D and Poppe B 2015 Understanding the lateral dose response functions of high-resolution photon detectors by reverse Monte Carlo and deconvolution analysis *Phys. Med. Biol.* **60** 6585-6607

McKerracher C and Thwaites D I 1999 Assessment of new small-field detectors against standard-field detectors for practical stereotactic beam data acquisition *Phys. Med. Biol.* **44** 2143-60

Morales J, Butson M, Crowe S B, Hill R and Trapp J V 2016 An experimental extrapolation technique using the Gafchromic EBT3 film for relative output factor measurements in small x-ray fields *Med. Phys.* **43** 4687-4692

Rogers D W O, Kawrakow I, Seuntjens J P, Walters B R B and Mainegra-Hing E 2011b *NRCC Report No. PIRS 702 rev C: NRC User Codes for EGSnrc* (Ottawa: National Research Council of Canada)

Rogers D W O, Walters B and Kawrakow I 2011a *NRCC Report No. PIRS 0509(A) rev L; BEAMnrc Users Manual* (Ottawa: National Research Council of Canada)

Scott A J D, Nahum A E and Fenwick J D 2008 Using a Monte Carlo model to predict dosimetric properties of small radiation fields. *Med. Phys.* **35** 4671-4684

Scott A J D, Nahum A E and Fenwick J D 2012 Characterizing the influence of detector density on dosimeter response in non-equilibrium small photon fields *Phys. Med. Biol.* **57** 4461–76

Sternheimer R M, Berger M J and Seltzer S M 1984 Density effect for the ionization loss of charged particles in various substances *At. Data Nucl. Data Tables* **30** 261-271

Underwood T S A, Winter H C, Hill M A and Fenwick J D 2013a Mass-density compensation can improve the performance of a range of different detectors under non-equilibrium conditions *Phys. Med. Biol.* **58** 8295-8310

Underwood T S A, Winter H C, Hill M A and Fenwick J D 2013b Detector density and small field dosimetry: Integral versus point dose measurement schemes. *Med. Phys.* **40** 082102-1-15

Underwood T S A, Thompson J, Bird L, Scott A J D, Patmore P, Winter H C, Hill M A and Fenwick J D 2015a Validation of a prototype DiodeAir for small field dosimetry *Phys. Med. Biol.* **60** 2939-2953

Underwood T S A, Rowland B C, Ferrand R and Vieillevigne L 2015b Application of the Exradin W1 scintillator to determine Ediode 60017 and microDiamond 60019 correction factors for relative dosimetry within small MV and FFF fields *Phys. Med. Biol.* **60** 6669-6683

Wulff J, Zink K and Kawrakow I 2008 Efficiency improvements for ion chamber calculations in high energy photon beams *Med. Phys.* **35** 1328-1336

Figure 1. Factors for the sequential conversion of mean dose in the detector sensitive volume to dose at a point in water, via electron particle fluences ϕ in the sensitive volume and intermediate structures.
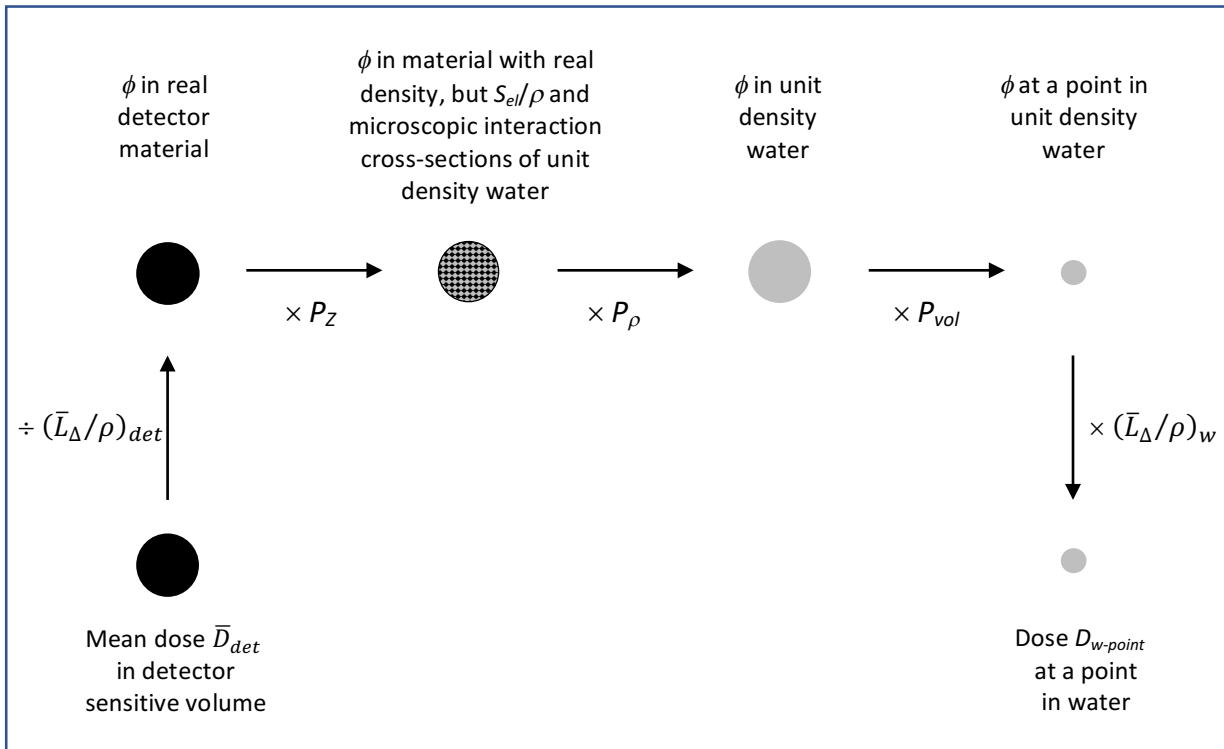
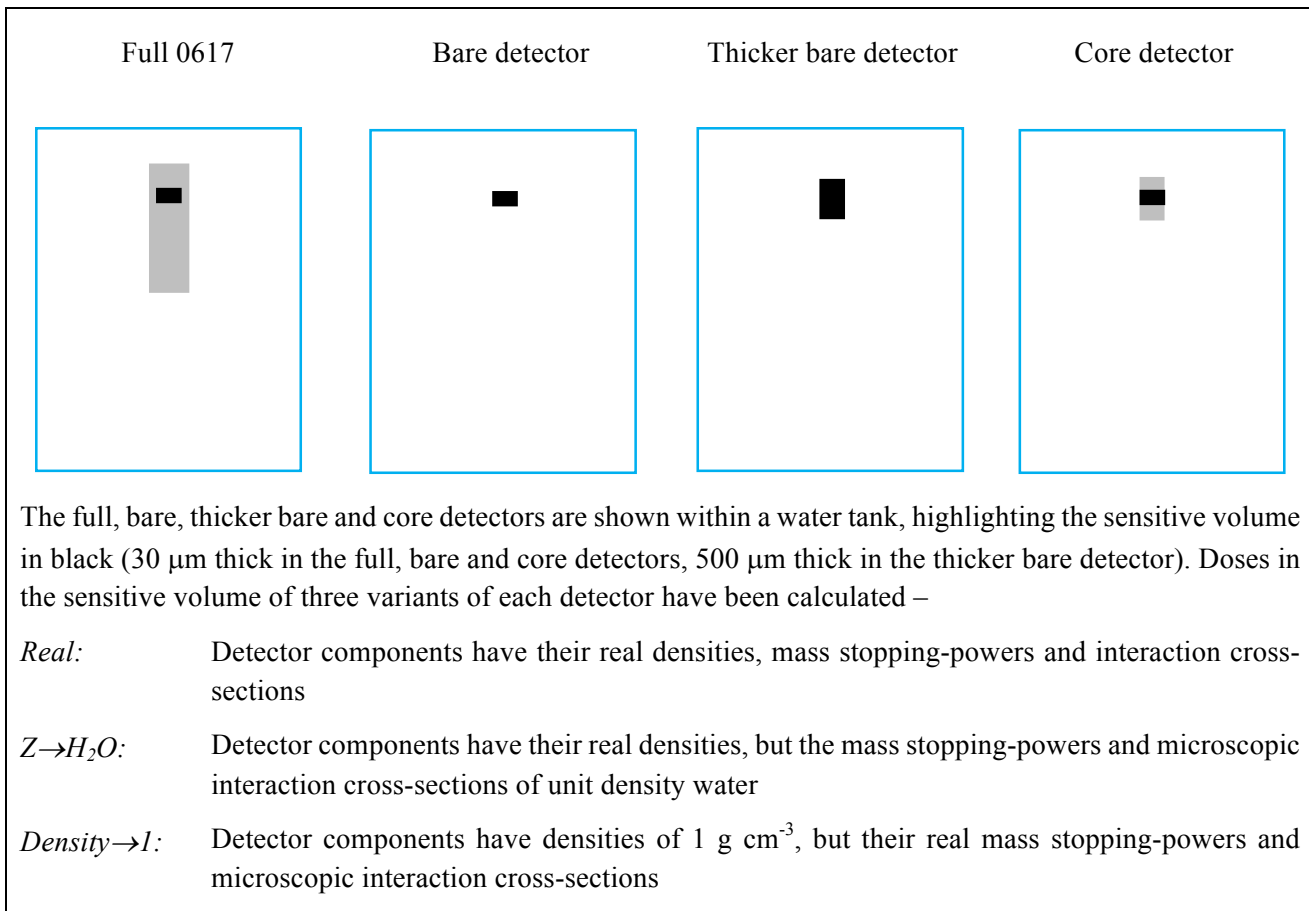Figure 2. Schematic summary of the detector geometries and material properties studied.

Full 0617	Bare detector	Thicker bare detector	Core detector

The full, bare, thicker bare and core detectors are shown within a water tank, highlighting the sensitive volume in black (30 μm thick in the full, bare and core detectors, 500 μm thick in the thicker bare detector). Doses in the sensitive volume of three variants of each detector have been calculated –

Real: Detector components have their real densities, mass stopping-powers and interaction cross-sections

Z→H₂O: Detector components have their real densities, but the mass stopping-powers and microscopic interaction cross-sections of unit density water

Density→1: Detector components have densities of 1 g cm^{-3}, but their real mass stopping-powers and microscopic interaction cross-sections

Figure 3. k correction factors calculated for real, $Z \rightarrow H_2O$ and density$\rightarrow 1$ variants of detectors, plotted with $\pm$ 2 s.d. confidence intervals.

a) 6 MV $k_{Q_{0.5,4\,cm}}^{0.5,4\,cm}$ factors for the fully modelled, core, thicker bare and bare versions of the 60017 diode detector aligned with the beam axis.
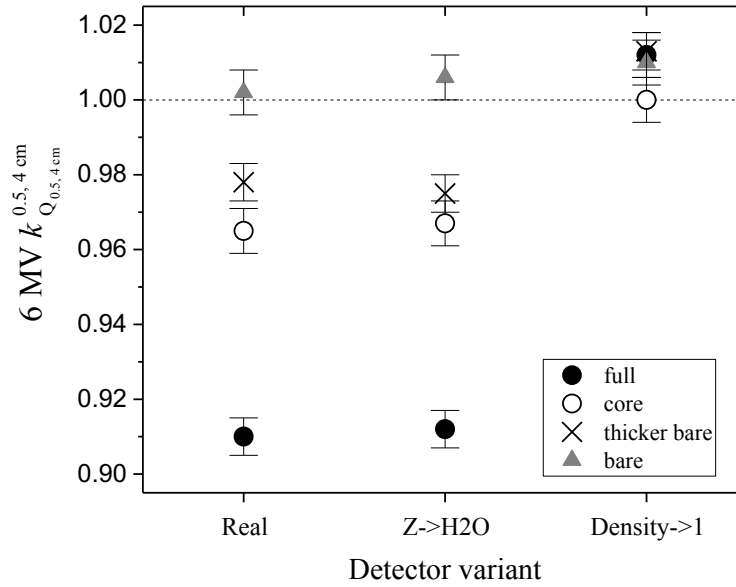
b) 6 MV $k_{Q_{0.7,4\,cm}}^{0.7,4\,cm}$, 6 MV $k_{Q_{0.5,4\,cm}}^{0.5,4\,cm}(45°)$ and 15 MV $k_{Q_{0.5,4\,cm}}^{0.5,4\,cm}$ factors for the fully modelled 60017 detector located on-axis.
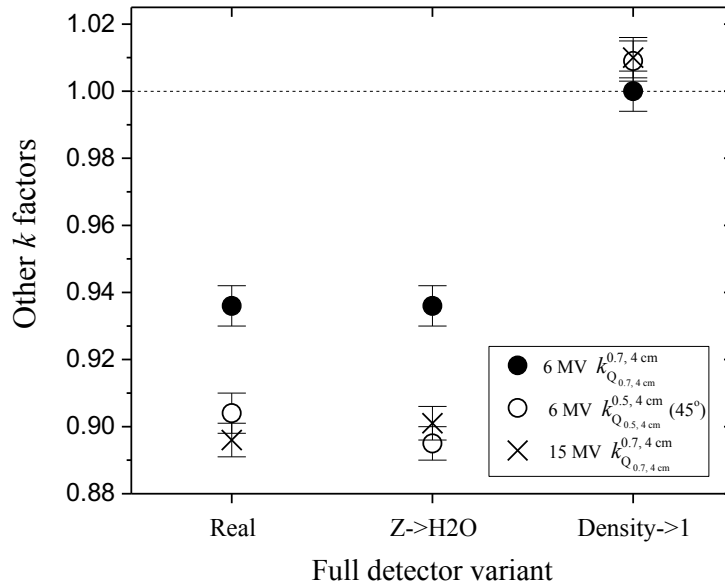
Figure 4. (a) P_{ρ} and (b) P_Z fluence perturbation factors calculated for the fully modelled, core, thicker bare and bare detectors aligned with the beam axis in 6 MV 0.5×0.5 and 4×4 cm^2 fields, plotted with ± 2 s.d. confidence intervals.

(a)
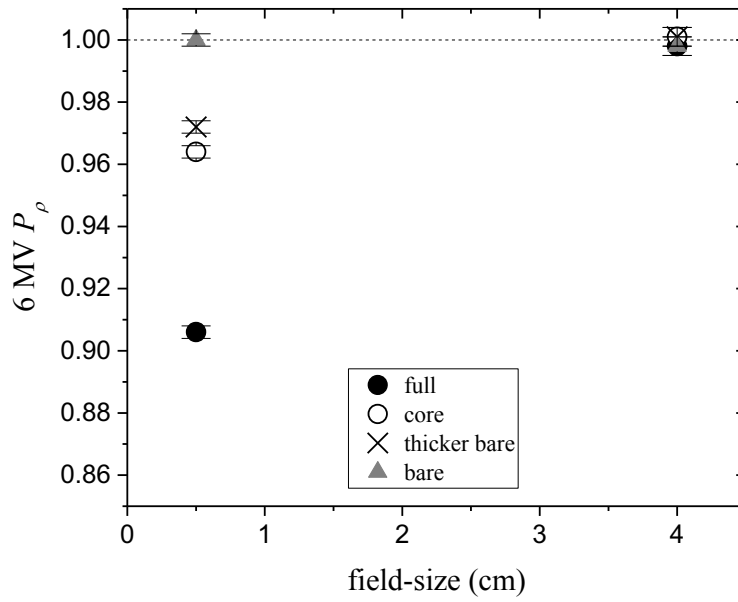
(b)
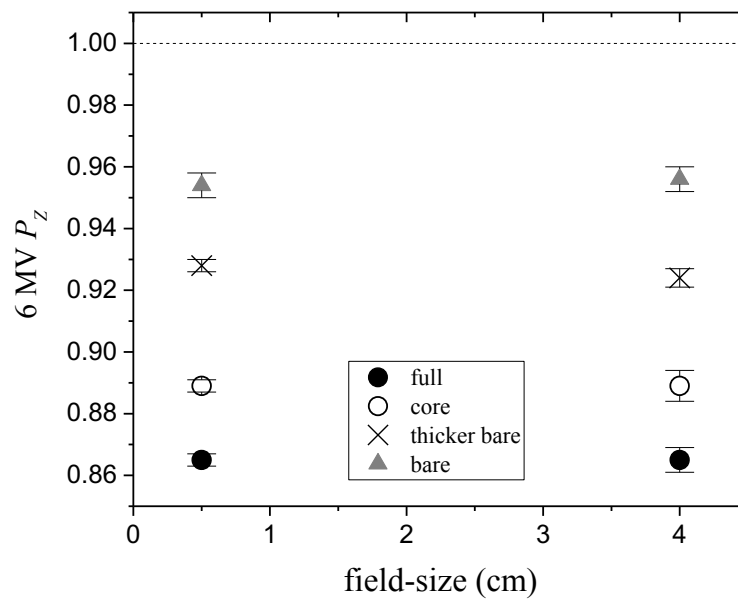
Figure 5. (a,b) Total electron (+ positron) fluence spectra in water and within the sensitive volumes of the real, density→1 and Z→H_2O variants of the core detector, aligned with the 6 MV beam axis in (a) 0.5×0.5 and (b) 4×4 cm^2 fields with the sensitive volume located at 5 cm depth in water set up at 100 cm SSD. (c,d) Ratios of the fluence spectra in water and in the sensitive volumes of the density→1 and Z→H_2O variants of the core detector to that in the real core detector, in 6 MV (c) 0.5×0.5 and (d) 4×4 cm^2 fields.

a)

b)

c)

d)
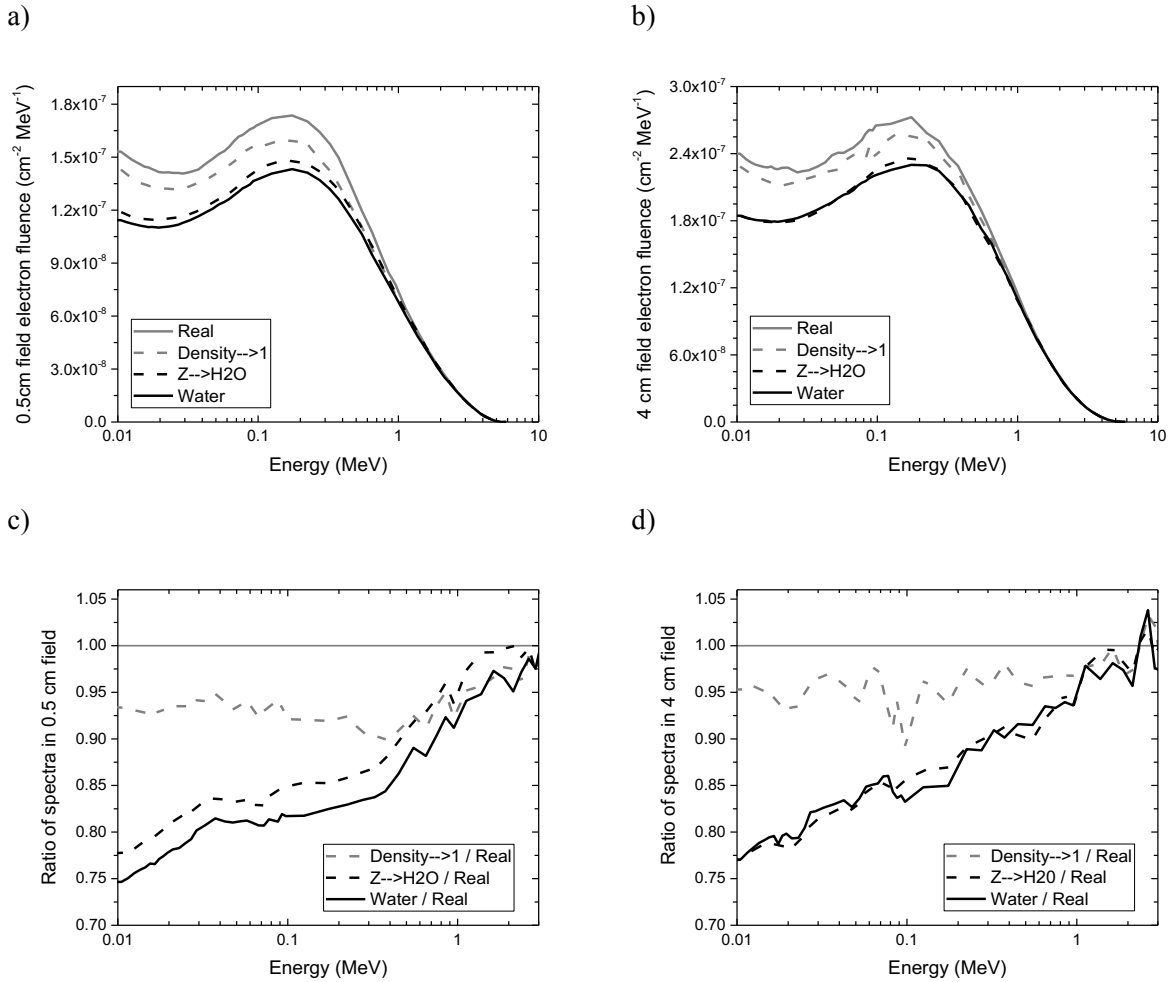
Figure 6. (a) The ratio of total electron (+ positron) fluence spectra in the sensitive volumes of the $Z{\rightarrow}H_2O$ and real core detectors for the 6 MV $0.5{\times}0.5$ cm^2 field, divided by the same ratio for the $4{\times}4$ cm^2 field, $[\phi_{E,core-Z{\rightarrow}H_2O}^{0.5\ cm}/\phi_{E,core}^{0.5\ cm}]/[\phi_{E,core-Z{\rightarrow}H_2O}^{4\ cm}/\phi_{E,core}^{4\ cm}]$. (b) The ratio of fluence spectra in water and in the $Z{\rightarrow}H_2O$ core detector sensitive volume for the 6 MV $0.5{\times}0.5$ cm^2 field, divided by the same ratio for the $4{\times}4$ cm^2 field, $[\phi_{E,w-sensvol}^{0.5\ cm}/\phi_{E,core-Z{\rightarrow}H_2O}^{0.5\ cm}]/[\phi_{E,w-sensvol}^{4\ cm}/\phi_{E,core-Z{\rightarrow}H_2O}^{4\ cm}]$.
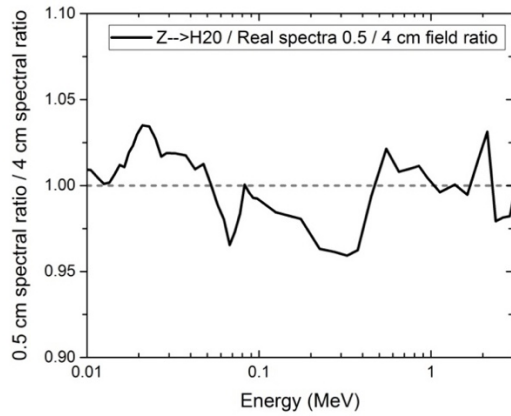
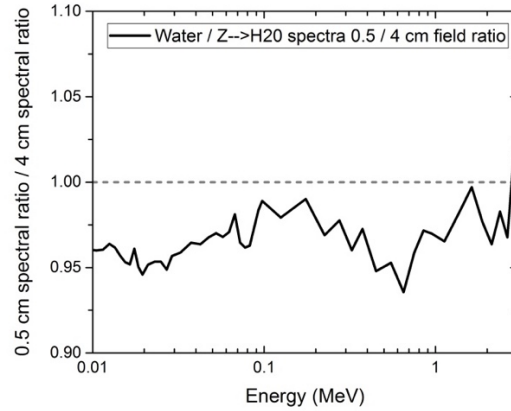a)   b)

Table 1. Computed doses absorbed by the sensitive volumes of the full, core, thicker bare and bare detectors, and their $Z{\rightarrow}H_2O$ and density$\rightarrow$1 variants, with the centre of the detector sensitive volume located on-axis at 5 cm depth in water in 6 MV 0.5×0.5 and 4×4 cm^2 fields and the detector aligned with the beam axis. Statistical uncertainties shown are $\pm$ 2 standard deviations (s.d.).

Field-size	0.5×0.5 cm^2	4×4 cm^2	0.5×0.5 cm^2	4×4 cm^2	0.5×0.5 cm^2	4×4 cm^2
Detector	Real		$Z{\rightarrow}H_2O$		Density$\rightarrow$1	
Dose absorbed by the sensitive volume per source particle (Gy × 10^{-17})						
Full	6.34 ± 0.01	9.01 ± 0.03	6.97 ± 0.01	9.91 ± 0.03	5.53 ± 0.01	8.74 ± 0.03
Core	5.81 ± 0.01	8.75 ± 0.04	6.55 ± 0.01	9.89 ± 0.04	5.43 ± 0.01	8.47 ± 0.03
Thicker bare	5.52 ± 0.01	8.44 ± 0.02	6.51 ± 0.01	9.91 ± 0.02	5.23 ± 0.01	8.28 ± 0.02
Bare	5.22 ± 0.01	8.16 ± 0.03	6.32 ± 0.01	9.92 ± 0.03	5.10 ± 0.01	8.05 ± 0.03

Table 2. Computed doses absorbed from the 6 MV 0.5×0.5 cm^2 field by a point-like cuboidal 0.25×0.25×0.5 mm^3 water voxel and a cylindrical water voxel of cross-section 1 mm^2 and thickness 0.5 mm, both centred on-axis at 5 cm deep in water in the absence of the detector, together with the dose absorbed from the 6 MV 4×4 cm^2 field by a co-located 2×2×0.5 mm^3 cuboidal voxel, which can be considered point-like in this wider field. Also tabulated are calculated water-to-silicon restricted mass stopping-power ratios $[\bar{L}_{10\text{ keV}}/\rho]_{Si}^{w}$ averaged over the electron spectra generated within the cylindrical water voxel by the 6 MV 0.5×0.5 and 4×4 cm^2 fields. Uncertainties are shown at the ± 2 s.d. level.

Voxel shape & cross-section	Cuboidal, point-like	Cylindrical, 1 mm^2	Cylindrical, 1 mm^2
	In-water dose per source particle (Gy × 10^{-17})		Stopping-power ratio $[\bar{L}_{10\text{ keV}}/\rho]_{Si}^{w}$
0.5×0.5 cm^2 field	6.35 ± 0.02	6.32 ± 0.01	1.2694 ± 0.0002
4.0×4.0 cm^2 field	9.92 ± 0.03		1.2715 ± 0.0002

Table 3. k correction factors calculated for the 60017 diode detector and its $Z{\rightarrow}H_2O$ and density$\rightarrow$1 variants positioned on-axis at 5 cm depth in water. 6 MV $k_{Q_{0.5,4\text{ cm}}}^{0.5,4\text{ cm}}$ factors are listed for the fully modelled, core, thicker bare and bare versions of the detector. Additionally, 6 MV $k_{Q_{0.5,4\text{ cm}}}^{0.5,4\text{ cm}}$ (45°), 6 MV $k_{Q_{0.7,4\text{ cm}}}^{0.7,4\text{ cm}}$ and 15 MV $k_{Q_{0.5,4\text{ cm}}}^{0.5,4\text{ cm}}$ factors are listed for the fully modelled version of the detector. Uncertainties are shown at the $\pm$ 2 s.d. level.

Correction factor	Detector	Real	$Z{\rightarrow}H_2O$	Density$\rightarrow$1
6 MV $k_{Q_{0.5,4\text{ cm}}}^{0.5,4\text{ cm}}$	Full	0.910 ± 0.005	0.912 ± 0.005	1.012 ± 0.006
6 MV $k_{Q_{0.5,4\text{ cm}}}^{0.5,4\text{ cm}}$	Core	0.965 ± 0.006	0.967 ± 0.006	1.000 ± 0.006
6 MV $k_{Q_{0.5,4\text{ cm}}}^{0.5,4\text{ cm}}$	Thicker bare	0.978 ± 0.005	0.975 ± 0.005	1.013 ± 0.005
6 MV $k_{Q_{0.5,4\text{ cm}}}^{0.5,4\text{ cm}}$	Bare	1.002 ± 0.006	1.006 ± 0.006	1.010 ± 0.006
6 MV $k_{Q_{0.5,4\text{ cm}}}^{0.5,4\text{ cm}}$ (45°)	Full	0.904 ± 0.006	0.895 ± 0.005	1.009 ± 0.006
6 MV $k_{Q_{0.7,4\text{ cm}}}^{0.7,4\text{ cm}}$	Full	0.933 ± 0.006	0.936 ± 0.006	1.000 ± 0.006
15 MV $k_{Q_{0.5,4\text{ cm}}}^{0.5,4\text{ cm}}$	Full	0.896 ± 0.005	0.901 ± 0.005	1.010 ± 0.006

Table 4. Values of P_ρ and P_Z factors calculated for the 60017 detector aligned with the beam axis at 5 cm depth in water in 6 MV 0.5×0.5 and 4×4cm^2 fields, together with corresponding values for the core, thicker bare and bare versions of the detector. Uncertainties are shown at the ± 2 s.d. level.

Detector	$P_\rho^{0.5\,cm}$	$P_\rho^{4\,cm}$	$P_Z^{0.5\,cm}$	$P_Z^{4\,cm}$
Full	0.906 ± 0.002	0.998 ± 0.003	0.865 ± 0.002	0.865 ± 0.004
Core	0.964 ± 0.002	1.001 ± 0.003	0.889 ± 0.002	0.889 ± 0.005
Thicker bare	0.972 ± 0.002	1.001 ± 0.003	0.928 ± 0.002	0.924 ± 0.003
Bare	1.000 ± 0.002	0.998 ± 0.003	0.954 ± 0.002	0.956 ± 0.004

Table 5. Doses absorbed by the sensitive volumes of the full detector and its $Z \rightarrow H_2O$ and density$\rightarrow$1 variants, with the centre of the sensitive volume located on-axis at 5 cm depth in water, and the detector aligned with the beam axis in a 6 MV 0.7×0.7 cm^2 field, at 45° to the axis in 6 MV 0.5×0.5 and 4×4 cm^2 fields, and aligned with the axis in 0.5×0.5 and 4×4 cm^2 15 MV fields. Associated doses absorbed in the absence of the detector by a point-like voxel of water located at 5 cm depth in the 6 MV 0.7×0.7 cm^2 and 15 MV 0.5×0.5 and 4×4 cm^2 fields are also shown. Uncertainties are shown at the ± 2 s.d. level.

Doses per source particle with the detector aligned with the axis of a 6 MV 0.7×0.7 cm^2 field			
Detector	Real	$Z \rightarrow H_2O$	Density$\rightarrow$1	Water
Dose (10^{-17} Gy)	7.24 ± 0.02	7.95 ± 0.02	6.55 ± 0.02	7.43 ± 0.03

Doses per source particle with the detector at 45° to the axis of 6 MV 0.5×0.5 and 4.0×4.0 cm^2 fields			
Detector	Real		$Z \rightarrow H_2O$	
Field-size	0.5×0.5 cm^2	4×4 cm^2	0.5×0.5 cm^2	4×4 cm^2
Dose (10^{-17} Gy)	6.23 ± 0.01	8.80 ± 0.03	7.09 ± 0.01	9.90 ± 0.03
Detector	Density$\rightarrow$1			
Field-size	0.5×0.5 cm^2	4×4 cm^2		
Dose (10^{-17} Gy)	5.45 ± 0.01	8.58 ± 0.03		

Doses per source particle with the detector aligned with the axis of 15 MV 0.5×0.5 and 4.0×4.0 cm^2 fields			
Detector	Real		$Z \rightarrow H_2O$	
Field-size	0.5×0.5 cm^2	4×4 cm^2	0.5×0.5 cm^2	4×4 cm^2
Dose (10^{-16} Gy)	3.36 ± 0.01	5.92 ± 0.01	3.71 ± 0.01	6.58 ± 0.02
Detector	Density$\rightarrow$1		Water	
Field-size	0.5×0.5 cm^2	4×4 cm^2	0.5×0.5 cm^2	4×4 cm^2
Dose (10^{-16} Gy)	2.86 ± 0.01	5.68 ± 0.02	3.34 ± 0.01	6.58 ± 0.02